Theoretical investigation of antisymmetric spin-orbit coupling effect on the physical properties of noncentrosymmetric BaPtSb superconductor

H. Y. Uzunok[a,b], H. M. Tütüncü[a,b], Ertuğrul Karaca[b], and G. P. Srivastava[c]

[a] *Sakarya Üniversitesi, Fen-Edebiyat Fakültesi, Fizik Bölümü, 54187, Adapazarı, Turkey*

[b] *Sakarya Üniversitesi, BIMAYAM, Biyomedikal, Manyetik ve Yarıiletken Malzemeler Araştırma Merkezi, 54187, Sakarya , Turkey*

[c] *School of Physics, University of Exeter, Stocker Road, Exeter EX4 4QL, UK*

Abstract

First principles pseudopotential calculations have been performed to explore the effect of spin-orbit coupling on the electronic, elastic, mechanical, vibrational and electron-phonon interaction properties of noncentrosymmetric BaPtSb crystallizing in the hexagonal SrPtSb-type. This coupling makes only moderate changes to the elastic and mechanical properties but significant changes to the phonon spectrum in the acoustic range. Analysis of the Eliashberg spectral function reveals that these low-frequency phonon modes originate from the vibrations of Pt and Sb atoms and couple strongly to their d and p electronic states at the Fermi level. The spin-orbit coupling has a significant effect on the electron-phonon interaction properties by decreasing the frequencies of some phonon modes and increasing the strength of the most dominant peak of the Eliashberg spectral function. The average electron-phonon coupling increases from 0.617 without spin-orbit coupling to 0.629 with spin-orbit coupling, resulting in the corresponding changes to the superconducting transition temperature from 1.46 to 1.54 K. The latter value of superconducting transition temperature compares very well with its experimental value of 1.64 K.

Key words: A. intermetallics; B.density functional theory,electronic structure, superconducting properties; E. abinitio calculations, physical properties

[1] Corresponding Author: H. M. Tütüncü Tel: +90 264 295 60 72 Fax: +90 264 295 59 50 e-Mail: tutuncu@sakarya.edu.tr

1 Introduction

Noncentrosymmetric superconductors (NCS), whose crystal structures do not possess inversion symmetry, are recently drawing attention because of their potential to exhibit unconventional superconductivity [1]. The lack of inversion symmetry in a crystal structure causes an electric field gradient parallel to the NCS crystal axis, resulting in antisymmetric spin-orbit coupling (ASOC). This coupling removes the spin degeneracy of the conduction bands and allows for superconducting states which are an admixture of spin-singlet and spin-triplet pairing, inducing a variety of exotic properties [1–4]. The finding of $CePt_3Si$ with the $CePt_3B$-type structure as the first noncentrosymmetric heavy fermion superconductor, presented evidence of spin-triplet Cooper pairs in the superconducting condensate [5]. Furthermore, the theoretically detected triplet component in the superconducting condensate was also experimentally demonstrated for $CeRhSi_3$, $CeIrSi_3$ and UIr [6]. However, these NCS materials display strong electronic correlations, thus the effect of ASOC on the existence of unconventional superconductivity is not definite. In order to find the role of ASOC in the emergence of unconventional superconductivity, it is required to explore new NCSs without strong correlations among electrons. Indeed, several weakly correlated NCSs have been discovered such as $LaPdSi_3$ [7], $LaPtSi_3$ [7], $LaIrSi_3$ [8], $LaRhSi_3$ [9], $BaPtSi_3$ [10–12], $SrPtGe_3$ [13], $SrPdGe_3$ [13], $CaIrSi_3$ [14], $CaPdSi_3$ [14], and $SrAuSi_3$ [15]. Although these NCSs do not contain f-shell, the existence of d states in them could reveal that their electronic bands may be influenced by the inclusion of SOC. Experimental studies on these NCSs have indicated that most of them are conventional BCS-type superconductors.

The appearance of superconductivity in f-shell free NCS materials has stimulated theoretical studies on their physical properties. The SOC effect on the electronic and vibrational properties of $BaPtSi_3$ [10] has been studied utilizing the density functional theory within the local density approximation (LDA). This work reveals that the splitting of electronic bands near the Fermi level is negligible. Thus, Bauer and co-workers have deduced that superconductivity in $BaPtSi_3$ connects to a virtually undisturbed BCS state [10]. Ab initio full-potential-linearised augmented plane wave (FLAPW) calculations [16] have been performed to examine the structural and electronic properties of NCSs $CaIrSi_3$ and $CaPdSi_3$. For both NCSs, the density of states at the Fermi lelvel is dominated by transition metal d states with an admixture of Si p states [16]. The overall influence of noninversion symmetry appears to be of trivial significance for the electronic properties of these NCSs [16]. Terashima and co-workers [17] have carried out angle-resolved de Hass-van Alphen (dHvA) measurements and FLAPW band-structure calculations for $LaRhSi_3$. Their work [17] suggested that the dHvA frequency branches found in this noncentrosymmetric superconductor could quantitatively be explained by the calculated Fermi surface, which consists of three pairs of inversion-asymmetry-split sheets. A full-potential local-orbital method [18] has been employed to examine the electronic properties of $LaPdSi_3$. This theoretical [18] work reveals that the SOC makes little influence on the density of states around the Fermi level. The electron-phonon interaction properties of NCS $SrAuSi_3$ and $CaIrS_3$ have been examined utilizing first

principles density functional calculations within the generalized gradient approximation [19,20]. These theoretical works [19,20] reveal that the influence of SOC on the electron-phonon properties remains rather small. Recently, we have presented the role of SOC in the physical properties of the La-based NCS using the *ab initio* pseudopotential method [21]. This theoretical work [21] finds that SOC has more effect on the physical properties of $LaIrSi_3$ rather than that of $LaRhSi_3$ (or $LaPdSi_3$) associated with the heavier mass of Ir atom than that of Rh atom (or Pd atom). As a consequence, theoretical studies mentioned above confirm that these NCSs are conventional BCS-tpye superconductors with weak electron-phonon interaction.

Very recently, the equatomic ternary compound BaPtSb has been reported to display superconductivity at 1.64 K [22]. This superconductor adopts the hexagonal SrPtSb-type crystal structure [23], which is shown in Fig. 1. This is a ternary ordered variant of the hexagonal AlB_2-type structure. We have to mention that the well-known high temperature superconductor MgB_2 also adopts the hexagonal AlB_2-type structure, where Boron atoms constitute a primitive honeycomb lattice consisting of graphite-like sheets separated by hexagonal layers of Mg atoms. In BaPtSb, the Sr atom is located at the Al atomic site while the Pt and Sb atoms successively are located the B atomic site, building a PtSb ordered honeycomb network. As can be seen from Fig. 1, the honeycomb sheets are arranged along the z-axis and thus spatial inversion symmetry is violated intrinsically. As a result, BaPtSb is a noncentrosymmetric superconductor, characterised with strong spin orbit coupling of Pt and Sb. Thus, BaPtSb is an excellent choice to analyze the effect of spin-orbit coupling on the its physical properties such as electronic, elastic, mechanical, vibrational and electron-phonon interaction.

This work is aimed to analyze the influence of SOC on the physical properties of BaPtSb, such as electronic, elastic, mechanical, vibrational and electron-phonon interaction; these are special properties which have not been examined before. We have presented our calculated results of the electronic, elastic and mechanical properties using the *ab inito* pseudopotential method based on a generalized gradient approximation (GGA) of the density functional theory (DFT) with and without the SOC [24,25]. An *ab initio* linear response method is utilized to investigate phonon dispersion relations and electron-phonon interaction properties of this non-centrosymmetric superconductor. The effect of SOC on the electron-phonon coupling strength (λ) as well as the superconducting transition temperature (T_c) has been examined.

2 Method

We performed first principles calculations, based on the DFT, using the computer package QUANTUM ESPRESSO [24,25]. The exchange correlation energy has been determined using the GGA with Perdew-Burke-Ernzerhof scheme (PBE) [26]. The ionic cores has been represented by full relativistic ultra-soft potentials for Ba, Pt and Sb atoms [27]. SOC is included in all calculations. The electronic wave functions

have been expanded in a plane-wave basis set with energy cut-off 60 Ry. For the sampling of the Brillouin zone, we have utilized a 8×8×8 and 24×24×24 $\boldsymbol{k}$-point grid generated according to the Monkhorst-Pack scheme [29] for structural and electronic properties, respectively.

In this study, the second order elastic constants have been computed by using strain-stress method. The details of the calculations can be found in the theoretical work of Farst and co-workers [30]. By incorporating small strains to the equilibrium lattice, we obtained the resulting change in the total energy, and from this information derived single crystal elastic constants of BaPtSb. There are five linearly independent elastic constants for a hexagonal system, C_{11}, C_{12}, C_{13} and C_{44} ($C_{44} = C_{55}$). The sixth one C_{66} is equal to $\frac{1}{2}(C_{11}\text{-}C_{12})$.

The phonon frequencies and polarization vectors are calculated using linear-response theory [24,25]. The Brillouin-zone integration during linear-response calculations are realized using a 8×8×8 $\boldsymbol{k}$-point grid [24,25]. The dynamical matrices are calculated on a 4×4×4 $\boldsymbol{q}$-point grid, resulting in 12 irreducible $\boldsymbol{q}$ points. Then, they are Fourier-transformed to real space and thus the force constants are obtained which can be used to determine phonon frequencies for any chosen $\boldsymbol{q}$-points.

Electron-phonon interaction calculations have been made using the Migdal-Eliashberg theory and linear-response theory together [24,25,31,32]. The technique for the calculation of the electron-phonon interaction has been explained in detail in our previous study [33]. Fermi-surface sampling for the evaluation of the electron-phonon matrix elements has been made using the 24×24×24 $\boldsymbol{k}$-mesh with a Gaussian width of 0.02 Ry. The phonon density of states and the Eliashberg function have been also worked out using this $\boldsymbol{k}$-mesh.

3 Results

3.1 Equilibrium structure and Electronic Properties

BaPtSb adopts the hexagonal SrPtSb-type crystal structure lacking inversion symmetry, with space group P$\bar{6}$m2, and one formula unit per primitive unit cell [22,23], as shown in Fig. 1. There are three atoms in the primitive unit cell, with their Wyckoff positions as Ba (1a) (0, 0, 0), Pt (1d) (1/3, 2/3, 1/2) and Sb (1f) (2/3, 1/3, 1/2). A set of total energy calculations versus cell volume has been performed in order to define the equilibrium volume, the bulk modulus B and the pressure coefficient $B^{'}$. Then, at the equilibrium volume, the final values of the lattice constants a and c/a are obtained by making total energy calculations. Tab. 1 provides the calculated values of a, c, B and $B^{'}$, along with available experimental data for the lattice parameters [23]. The variation from the experimental values of a and c is less than 2%. We are not aware of any experimental data for the values of B and $B^{'}$.

We have presented the influence of SOC on the electronic structure in Fig. 2 (a). The

electronic structure shows metallic character with Sn p-like bands, admixed with the transition metal d bands, crossing the Fermi level. As seen in Fig. 1, the inversion symmetry in BaPtSb is ruined by the arrangement of atoms along the [010] and [001] directions (see Fig. 1). As a consequence, the double degeneracy of electronic bands is still present along the Γ-M ([010]) and Γ-A ([010]) symmetry directions because the asymmetric spin-orbit coupling (ASOC) can be seen only perpendicular to the directions which break inversion symmetry as depicted in Fig. 2 (a). [PLEASE check the previous two sentences and modify if necessary.] In order to identify the specific electronic states connected with superconductivity, the total and partial density of states (PDOS) are calculated and presented in Fig. 2 (b). The PDOS reveals that the effect of Ba atoms on superconductivity can be ruled out since the Ba-like DOS close to the Fermi level is very small and featureless. This result is not surprising because Ba element is almost in the form of cation Ba^{2+} and behaves like an electron donor. This fact indicates the picture of a charge transfer from Ba atom to the PtSb honeycomb lattice. Thus, the observed superconductivity in BaPtSb seems to be an intrinsic feature of the PtSb honeycomb lattice while Ba electronically stabilizes the crystal structure. The PDOS curves conspicuously reveal the hybridization between Sn 5p and Pt 5d states near the Fermi level. The value of $N(E_F)$ is calculated to be 1.87 States/eV which decreases to 1.80 State/eV by turning off the SOC. The value of $N(E_F)$ consists of roughly 1% Ba electronic states, 47% Pd electronic states and 52% Sn electronic states. In particular, Pt 5d and Sn 5p states alone contribute to $N(E_F)$ up to 36% and 51% respectively. This result suggests that these electrons are most influential in developing the superconducting properties of BaPtSb.

The horizontal ASOC splitting of the electronic bands around E_F is an important feature for defining superconductivity in NCS compounds. As can be seen from Fig. 2(a), the horizontal ASOC splittings at E_F along the high symmetry points such as Γ-K, K-M, and A-H are distinguishable which could cause splitting in the Fermi surfaces. To recognize these splittings, we have illustrated the Fermi surfaces of with (on the right) and without (on the left) SOC in Fig. 3. It is clear that the Fermi surfaces are divided into split sheets because of ASOC. Especially near the zone boundary, the splitting due to the ASOC is quite effective as can be seen at the K high symmetry point in Fig. 2(a). The inner cylindrical Fermi surface is not affected greatly by the onset of SOC because there is negligible splitting around the zone center electronic bands. Even though the Fermi surfaces have been separated, the intersection between the split surfaces is rather small. Thus we can say that there the superconducting phase is more spin-singlet pairing type rather than the spin-triplet pairing type.

3.2 Elastic and Mechanical Properties

The calculated values of single crystal elastic constants for BaPtSb with and without SOC are given in Tab. 2. Unfortunately, there are no theoretical and experimental results to compare our results with. When SOC is included, the values of single crystal elastic constants do not change by more than 5%. This maximum change suggests that SOC makes a small influence on the values of elastic constants. Thus, SOC is

expected to make the same level of effect on the phonon properties of BaPtSb because elastic constants are associated with many physical properties like inter-atomic potentials, equation of state and phonon spectrum. From the calculated values of single crystal elastic constants, we can assess the intrinsic mechanical stability of the noncentrosymmetric superconductor studied. The condition for mechanical stability of hexagonal crystals is presented by the following conditions:

$$C_{44} > 0; \qquad C_{11} > |C_{12}|; \quad \text{and} \quad (C_{11} + 2C_{12})C_{33} > 2C_{13}.$$

The both calculated values of C_{ij} with and without SOC meet these criteria, indicating that the noncentrosymmetric superconductor studied is mechanically stable. In Tab. 2, the calculated value of C_{33} is much smaller than that of C_{11}. This observation indicates that the c-axis is more compressible than a axis. In other words, the bonding strength along the a axis is much larger than that along the c axis.

After obtaining the values of single crystal elastic constants, the isotropic bulk modulus (B_{VRH}), the isotropic shear modulus (G_{VRH}), Poisson's ratio (ν) and Young's modulus (E) can be derived by using the Voigt–Reuss–Hill (VRH) scheme [36–38]. The obtained values of the isotropic bulk modulus B_{VRH}, shear modulus G_{VRH}, Young's modulus E (all in GPa), B_H/G_H ratio and Poisons's ratio ν with and without SOC for BaPtSb are presented in Tab. 3. When SOC is considered, the values of above quantities do not change by more than 8%. In the light of this variation, we can propose that SOC has an intermediate-level of effect on the values of the above quantities due the small effect of SOC on the single crystal elastic constants. As given in Tab. 1, the value of bulk modulus from the equation of state is found to be 53.0 GPa which is comparable with the value of B_H derived from the single crystal elastic constants revealing the accuracy of the present investigations. The ratio between the bulk and shear modulus (B_H/G_H) is suggested by Pugh to foresee brittle or ductile behavior of materials [39]. According to the Pugh criterion [39], a material is ductile (brittle) if this ratio is greater (less) than a critical value of 1.75. The value of B_H/G_H for BaPtSb is found to be 2.66 with SOC and 2.51 without SOC which are both greater than the critical value of 1.75. Therefore, the noncentrosymmetric BaPtSb superconductor is inclined to exhibit ductile behavior. The Poisson's ratio provides information about the bonding properties of materials. The value of this ratio is around 0.1, 0.25 and 0.33 for covalent, ionic and metallic materials, respectively [40]. The value of this ratio for BaPtSb with SOC is equal to 0.33 which suggest that this noncentrosymmetric superconductor exhibits the metallic behavior.

The calculated values of B_H and G_H allow us to derive the transverse (V_T), longitudinal (V_L) and mean sound (V_M) elastic wave velocities :

$$V_T = \left(\frac{G_H}{\rho}\right)^{1/2} \tag{1}$$

$$V_L = \left(\frac{3B_H + 4G_H}{3\rho}\right)^{1/2} \tag{2}$$

$$V_m = \left[\frac{1}{3}\left(\frac{2}{V_T^3} + \frac{1}{V_L^3}\right)\right]^{-1/3}, \tag{3}$$

$$\tag{4}$$

where ρ refers to the mass density of the material. After obtaining the value of V_M, the Debye temperature Θ_D can be derived from the following equation [41]:

$$\Theta_D = \frac{h}{k}\left(\frac{3n}{4\pi}\frac{N_A\rho}{M}\right)^{1/3} V_m, \tag{5}$$

where k, h, n, N_A and M refer to the Boltzmann's constant, the Planck's constant, the number of atoms in the molecule, Avogadros number and the molecular weight, respectively. The determined values of V_T, V_L, V_M and Θ_D with and without SOC are given in Tab. 3. These quantities are slightly effected by the inclusion of SOC. The maximum variation has been observed for the value of V_T, and that is less than 4%. The calculated values of Θ_D compare well with the measured value of 186 K [22]. At low temperatures, the vibrational excitations originate only from acoustic vibrations. Therefore, at low temperatures, the Θ_D temperature derived from the elastic constants becomes comparable with that obtained from specific heat measurements [22].

3.3 Phonons and electron-phonon interaction

The zone-center phonon modes of BaPtSb can be classified by the irreducible representation of the point group D_{3h}. As obtained from group theory, the symmetries of the zone-center optical phonon modes can be presented as:

$$\Gamma(D_{3h}) = 2A_2^{''} + 2E^{'},$$

where $A_2^{''}$ modes are infrared active, and $E^{'}$ modes are Raman as well as infrared active. The eigendisplacements, frequencies and electron-phonon coupling parameters of these phonon modes for BaPtSb are presented in Fig. 4. The corresponding frequencies and electron-phonon coupling parameters without SOC are also given in the brackets. This figure reveals that the frequencies of these phonon modes do not change by more than 4% by the consideration of SOC. However, this coupling changes their electron-phonon coupling parameters up to around 30%. This result emphasizes that this coupling must be considered in order to define the superconducting properties of BaPtSb for good accuracy. The lower $A_2^{''}$ phonon mode arises from the opposing vibrations of Ba and Sb atoms against Pt along the [001] direction, with maximum contribution due to Pt atoms. The source of lower $E^{'}$ phonon mode is the opposing oscillations of three Ba atoms honeycomb lattices against two PtSb atoms honeycomb lattices along the [010] direction. The higher $A_2^{''}$ involves the opposing motion of Ba and Sb atoms along the [001] direction with Pt atoms being at rest. Finally, the higher $E^{'}$ phonon mode is formed by the opposing motion of Pt and Sb atoms in the [010] direction while Ba atoms are stationary.

The calculated phonon dispersion relations for BaPtSb with and without SOC are depicted in Fig. 5 (a). Both results with SOC and without SOC reveal the dynamical stability of BaPtSb in its noncentrosymmetric hexagonal SrPtSb-type crystal structure because all phonon branches possess real frequencies. The calculated phonon spectrum exhibits two distinct regions which are separated from each other by a gap of 1.4 THz due to the mass differences between three constituents. The low frequency region is composed of three acoustic and four optical branches extending up to 3.2 THz. All phonon bands in this region display significant amount of dispersion. There are two most remarkable features in this frequency region. Firstly, the upper-frequency acoustic modes interact with low-lying optical modes, resulting in an anticrossing feature. Secondly, the third highest mode shows strong softening along the A-H-L symmetry direction due to the consideration of SOC. [Huseyin, please check the above statement and let me know if you would prefer to change it.] We have to emphasize that this softening may play a substantial role in developing superconductivity in BaPtSb because a similar observation has been made for other superconductors [42–44]. The high frequency region of the phonon spectrum contains two optical phonon bands which exhibit a much reduced level of dispersion than the four optical phonon bands in the low-frequency region.

The phonon density of states and partial density of states presenting the frequency distribution of normal phonon modes are displayed in Fig. 5 (b). Movement implying the three different atomic types exist below the gap region. In particular, Pt vibrations are dominant below 1.8 THz while Ba vibrations are dominant between 1.8 and 2.5 THz. Above the phonon band gap, Sn vibrations are dominant because its atomic mass is the lightest. In order to examine a connection between the softening of the low-lying phonon modes and electron-phonon interaction, we have presented mode-dependent electron-phonon coupling parameter of this phonon branch ($\lambda_{\boldsymbol{q}j}$) with and without SOC in Fig. 6. The value of $\lambda_{\boldsymbol{q}j}$ will be effected by two quantities: the phonon frequency and electron-phonon coupling matrix elements. According to Eqs.**??** and **??**, the value of $\gamma_{\boldsymbol{q}j}$ does not depend on the phonon frequency. Thus, the value of λ changes mainly with $\frac{1}{\omega^2}$ according to Eq. **??**. As a consequence, the softening of the phonon branch upon the inclusion of SOC leads to a larger electron-phonon coupling parameter (see Fig. 5 (a) and Fig. 6). [As we have deleted some equations, reference to those equations is no longer valid. Please change text accordinly. Also, please check if Fig 6 refers to the LA branch or a LO branch.]

The Eliashberg spectral function $\alpha^2F(\omega)$ and the frequency variation of the average electron-phonon coupling parameter for BaPtSb are illustrated in Fig. 7. The corresponding results without SOC are also presented in this figure for comparison. Firstly, this figure reveals that the SOC makes a significant influence on the phonon and electron-phonon interaction properties of this noncentrosymmetric superconductor. This coupling reduces the frequency of some phonon modes and enhances the strength of the most dominant peak (at around 1.4 THz) of the Eliashberg spectral function. Thus, the value of λ increases from 0.617 to 0.629 with the inclusion of SOC. As a consequence, the SOC-related enhancement of the λ value for BaPtSb can be related to both a softening of its phonon spectrum and an increase

in its electron-phonon coupling matrix elements. Secondly, this spectral function reveals that in BaPtSb the scattering of near-Fermi level electrons from low-frequency phonons plays a dominant role in the transition from the normal state to the superconducting state because the vibrational phonon modes below 1.8 THz offer about 70% to λ. This result is totally expected because these phonon modes are due to the coupled motion of Pt and Sb atoms (see also a sharp peak at 1.4 THz in Fig. 5 (b)) which dominate the electronic states close to the Fermi level with their d and p states.

The Allen-Dynes modified McMillan equation [34,35] is usually utilized to estimate the superconducting transition temperature T_c:

$$T_c = \frac{\omega_{\ln}}{1.2} \exp\left(-\frac{1.04(1+\lambda)}{\lambda - \mu^*(1+0.62\lambda)}\right), \tag{6}$$

where μ^* is the Coulomb pseudopotential representing Coulombic repulsion. The value of μ^* is normally estimated to lie between 0.10 and 0.16. We utilized the average value of 0.13 for the calculation of T_c. Furthermore, the values of λ and $N(E_F)$ let us to obtain the electronic specific heat coefficient γ which is given as

$$\gamma = \frac{1}{3}\pi^2 k_B^2 N(E_F)(1+\lambda). \tag{7}$$

Finally, the calculated values of the physical quantities ($N(E_F)$, ω_{ln}, λ, γ, Θ_D and T_c) with and without SOC associated with superconductivity in the noncentrosymmetric BaPtSb superconductor are presented in Tab. 5. We have to mention that the presented values of Θ_D in this table are calculated using the quasi-static harmonic approximation [45,46]. The value of Θ_D is calculated to be 182 K without SOC and 184 K with SOC which both are comparable with the experimental value of 186 K [22]. In addition, both calculated values of γ are consistent with the experimental value of 6.86 $\frac{mJ}{molK^2}$ [22]. This table reveals that phonons in BaPtSb become slightly softer with the consideration of SOC. The values of λ and T_c increase from 0.617 to 0.629 and from 1.46 to 1.54 K, respectively. Thus, the inclusion of SOC makes the agreement between theory and experiment for the value of T_c slightly better.

4 Summary

We have presented *ab initio* results for the effect of spin-orbit coupling on the electronic, elastic, mechanical, vibrational and electron-phonon interaction properties of of BaPtSb which possesses the hexagonal SrPtSb-type crystal structure lacking inversion symmetry. The calculated electronic structure of this noncentrosymmetric superconductor reveals that the lack of inversion symmetry in its crystal structure gives rise to an antisymmetric spin-orbit coupling. Therefore, when SOC is considered, the double degeneracy of electronic bands is removed along all the considered symmetry directions, except the Γ-N ([010]) and Γ-A ([001]) symmetry directions.

Along these symmetry directions, the double degeneracy of electronic bands is not lifted since the ASOC exists only along perpendicular to the directions which break inversion symmetry.

The partial electronic DOS shows that the influence of Ba atoms on superconductivity can be ignored because the Ba-like DOS near the Fermi level is negligible. Thus, the observed superconductivity in the studied noncentrosymmetric superconductor appears to be an intrinsic property of the PtSb honeycomb lattice while the role of Ba is to electronically stabilize the crystal structure of BaPtSb. The calculated values of single crystal elastic constants confirms the mechanical stability of BaPtSb in its noncentrosymmetric SrPtSb-type crystal structure. SOC has a small effect on the values of these elastic constants with the maximum change not more than 5%. SOC makes an intermediate-level effect on the values of the shear modulus (G_{VRH}), Poisson's ratio (ν) and Young's modulus (E), with makes an intermediate effect on the values of above quantities with the maximum change not more than 8%. The ratio between the bulk modulus and shear modulus (B_H/G_H) indicates that the noncentrosymmetric BaPtSb superconductor is inclined to display ductile behavior.

The eigendisplacements, frequencies and electron-phonon coupling parameters of zone-center phonon modes for BaPtSb are presented and discussed in detail. A critical assessment of these phonon modes reveals that their frequencies do not change by more than 4% by the consideration of SOC, but this coupling has significant effect on their electron-phonon coupling parameters with the change up to around 30%. The most notable feature of calculated phonon spectrum is the softening of phonons in longitudinal acoustic range along the A-H-L symmetry directions when SOC is included. This softening raises the value of the electron-phonon coupling considerably because this parameter changes mainly with $\frac{1}{\omega^2}$. The calculated spectral Eliashberg spectral function indicates that the scattering of near Fermi-level electrons from low-frequency phonons plays a dominant role in the transition from the normal state to the superconducting state. This is because these phonon modes are due to the coupled motion of Pt and Sb atoms which dominate the states close to the Fermi level with their d and p states. SOC also makes a significant effect on the electron-phonon interaction properties of this noncentrosymmetric superconductor. This coupling decreases the frequency of some phonon modes and augments the strength of the most dominant peak of the Eliashberg spectral function of BaPtSb. Thus, this coupling increases the value of λ from 0.617 to 0.629. The SOC-related enhancement of λ value for BaPtSb has been linked to both a softening of its phonon spectrum and an increase in its electron-phonon coupling matrix elements. Finally, the calculated values of superconducting transition temperature, electronic specific heat coefficient and Debye temperature are in good accordance with their measured values.

References

[1] M. Smidman, M. B. Salamon, H. Q. Yuan, and D. F. Agterberg, Superconductivity and spin-orbit coupling in non-centrosymmetric materials: A review, Rep. Prog. Phys.

80 (2017) 036501.

[2] E. Bauer and M. Sigrist, Non-Centrosymmetric Superconductors: Introduction and Overview, Lecture Notes in Physics (Springer, 2012).

[3] L. P. Gorkov and E. I. Rashba, Superconducting 2D System with Lifted Spin Degeneracy: Mixed Singlet-Triplet State, Phys. Rev. Lett. 87 (2001) 037004.

[4] P. A. Frigeri, D. F. Agterberg, A. Koga, and M. Sigrist, Superconductivity without Inversion Symmetry: MnSi versus $CePt_3Si$, Phys. Rev. Lett. 92 (2004) 097001.

[5] E. Bauer, G. Hilscher, H. Michor, Ch. Paul, E. W. Scheidt, A. Gribanov, Yu. Seropegin, H. Nol, M. Sigrist, and P. Rogl, Heavy Fermion Superconductivity and Magnetic Order in Noncentrosymmetric $CePt_3Si$, Phys. Rev. Lett. 92 (2004) 027003.

[6] T. Akazawa, H. Hidaka, T. Fujiwara, T.C. Kobayashi, E. Yamamoto, Y. Haga, R. Settai, and Y. Onuki, Pressure-induced superconductivity in ferromagnetic UIr without inversion symmetry, J. Phys. Condens. Matter 16 (2004), pp. L29-L32.

[7] M. Smidman, A. D. Hillier, D. T. Adroja, M. R. Lees, V. K. Anand, R. P. Singh, R. I. Smith, D. M. Paul, G. Balakrishnan, Investigations of the superconducting states of noncentrosymmetric $LaPdSi_3$ and $LaPtSi_3$, Phys. Rev. B 89 (2014) 094509.

[8] V. K. Anand, D. Britz, A. Bhattacharyya, D. T. Adroja, A. D. Hillier, A. M. Strydom, W. Kockelmann, B. D. Rainford, K. A. McEwen, Physical properties of noncentrosymmetric superconductor $LaIrSi_3$: A μSR study, Phys. Rev. B 90 (2014) 014513.

[9] N. Kimura, N. Kabeya, K. Saitoh, K. Satoh, H. Ogi, K. Ohsaki and H. Aoki, Type II/1 Superconductivity with Extremely High Hc3 in Noncentrosymmetric $LaRhSi_3$, J. Phys. Soc. Jpn. 85 (2016) 024715.

[10] E. Bauer, R. T. Khan, H. Michor, E. Royanian, A. Grytsiv, N. Melnychenko-Koblyuk, P. Rogl, D. Reith, R. Podloucky, E.-W. Scheidt, W. Wolf, and M. Marsman, $BaPtSi_3$: A noncentrosymmetric BCS-like superconductor, Phys. Rev. B 80 (2009) 064504.

[11] R. Ribeiro-Palau, R. Caraballo, P. Rogl, E. Bauer, and I. Bonalde, Strong-coupling BCS superconductivity in noncentrosymmetric $BaPtSi_3$: a low-temperature study, J. Phys.: Condens. Matter 26 (2014) 235701.

[12] F. Kneidinger, E. Bauer, I. Zeiringer, P. Rogl, C. Blass-Schenner, D. Reith, R. Podloucky, Superconductivity in non-centrosymmetric materials, Phys. C 514 (2015) p. 388.

[13] F. Kneidinger, L. Salamakha, E. Bauer, I. Zeiringer, P. Rogl, C. Blaas-Schenner, D. Reith, and R. Podloucky, Superconductivity in noncentrosymmetric $BaAl_4$ derived structures, Phys. Rev. B 90 (2014) 024504.

[14] R. P. Singh, A. D. Hillier, D. Chowdhury, J. A. T. Barker, D. McK. Paul, M. R. Lees, and G. Balakrishnan, Probing the superconducting ground state of the noncentrosymmetric superconductors $CaTSi_3$ (T = Ir, Pt) using muon-spin relaxation and rotation, Phys. Rev. B 90 (2014) 104504.

[15] M. Isobe, M. Arai, and N. Shirakawa, Superconductivity in noncentrosymmetric $SrAuSi_3$, Phys. Rev. B 93 (2016) 054519.

[16] V. V. Bannikov, I. R. Shein, and A. L. Ivanovskii, Structural and electronic properties and the fermi surface of the new noncentrosymmetric superconductors: 3.6 K $CaIrSi_3$ and 2.3 K $CaPtSi_3$, JETP Lett. 92 (2010) 343.

[17] T. Terashima, M. Kimata, S. Uji, T. Sugawara, N. Kimura, H. Aoki, H. Harima, Fermi surface in $LaRhSi_3$ and $CeRhSi_3$, Phys. Rev. B 78 (2008) 205107.

[18] M.J. Winiarski, M. Samsel-Czekala, Electronic structure of noncentrosymmetric superconductor $LaPdSi_3$ and its reference compound $LaPdGe_3$, Intermetallics 56 (2015) 44-47.

[19] E. Arslan, E. Karaca, H. M. Tütüncü, A. Başoğlu, G. P. Srivastava, Theoretical investigation of superconductivity in $SrAuSi_3$ and $SrAu_2Si_2$, J. Phys. Chem. Solids 95 (2010) 65-73.

[20] H. Y. Uzunok, E. İpsara, H. M. Tütüncü, G. P. Srivastava, A. Başoğlu, The effect of spin orbit interaction for superconductivity in the noncentrosymmetric superconductor $CaIrSi_3$, J. Alloys Compd. 681 (2016) 205.

[21] H. Y. Uzunok, H. M. Tütüncü, G. P. Srivastava, E. İpsara, A. Başoğlu, The effect of spin orbit interaction on the physical properties of $LaTSi_3$ (T = Ir, Pd, and Rh): First-principles calculations, J. Appl. Phys. 121 (2017) 193904.

[22] K. Kudo , Y. Saito, T. Takeuchi, Shin-ya Ayukawa, T. Kawamata, S. Nakamura, Y. Koike, and M. Nohara, Superconductivity in BaPtSb with an Ordered Honeycomb Network, J. Phys. Soc. Jpn. 87 (2018) 063702.

[23] G. Wenski and A. Mewis,Trigonalplanar koordiniertes Platin: Darstellung und Struktur von SrPtAs (Sb), BaPtP(As, Sb), $SrPt_xP_{2x}$, $SrPt_xAs_{0,90}$ und $BaPt_xAs_{0,90}$, Z. Anorg. Allg. Chem. 535 (1986) 110.

[24] P. Giannozzi, S. Baroni, N. Bonini, M. Calandra, R. Car, C. Cavazzoni, D. Ceresoli, G. L. Chiarotti, M. Cococcioni, I. Dabo, A. Dal Corso, S. de Gironcoli, S. Fabris, G. Fratesi, R. Gebauer, U. Gerstmann, C. Gougoussis, A. Kokalj, M. Lazzeri, L. Martin-Samos, N. Marzari, F. Mauri, R. Mazzarello, S. Paolini, A. Pasquarello, L. Paulatto, C. Sbraccia, S. Scandolo, G. Sclauzero, A. P. Seitsonen, A. Smogunov, P. Umari, R. M. Wentzcovitch, QUANTUM ESPRESSO: a modular and open-source software project for quantum simulations of materials, J. Phys.: Condens. Matter 21 (2009) 395502.

[25] P. Giannozzi, O. Andreussi, T. Brumme, O. Bunau, M. Buongiorno Nardelli, M. Calandra, R. Car, C. Cavazzoni, D. Ceresoli, M. Cococcioni, N. Colonna, I. Carnimeo, A. Dal Corso, S. de Gironcoli, P. Delugas, R. A. DiStasio Jr., A. Ferretti, A. Floris, G. Fratesi, G. Fugallo, R. Gebauer, U. Gerstmann, F. Giustino, T. Gorni, J. Jia, M. Kawamura, H.-Y. Ko, A. Kokalj, E. Kkbenli, M. Lazzeri, M. Marsili, N. Marzari, F. Mauri, N. L. Nguyen, H.-V. Nguyen, A. Otero-de-la-Roza, L. Paulatto, S. Ponc, D. Rocca, R. Sabatini, B. Santra, M. Schlipf, A. P. Seitsonen, A. Smogunov, I. Timrov, T. Thonhauser, P. Umari, N. Vast, X. Wu, and S. Baroni, Advanced capabilities for materials modelling with Quantum ESPRESSO, J. Phy.: Condensed Matter 29 (2017) 465901.

[26] J. Perdew and A. Zunger, Self-interaction correction to density-functional approximations for many-electron systems, Phy. Rev. B 23 (1981) pp. 5048–5079.

[27] A. M. Rappe, K. M. Rabe, E. Kaxiras, and J. D. Joannopoulos, Optimized pseudopotentials, Phys. Rev. B 41 (1990) pp. 1227–1230 (R).

[28] W. Kohn and L. J. Sham, Self-Consistent Equations Including Exchange and Correlation Effects, Phys. Rev. 140 (1965) pp. A1133–A1138.

[29] H. J. Monkhorst and J. D. Pack, Special points for Brillonin-zone integrations, Phys. Rev. B 13 (1976) pp. 5188–5192.

[30] L Farst, J. M. Wills, B. Johansson and E. Erikson, Elastic constants of hexagonal transtion metal, Phys. Rev. B 51 (1995) pp. 17431–17438 (R).

[31] A. B. Migdal, Interaction between electrons and lattice vibrations in a normal metal, Zh. Eksp. Teor. Fiz. 34 (1958) pp. 996–1001.

[32] G. M. Eliashberg, Interaction between electrons and lattice vibrations in a superconductor, Sov. Phys. JETP. 11 (1960) pp. 696–702.

[33] H. M. Tütüncü, H. Y. Uzunok, Ertuğrul Karaca, G. P. Srivastava, S. Özer, and Ş. Uğur, Ab initio investigation of BCS-type superconductivity in $LuNi_2B_2C$-type superconductors, Phys. Rev. B 92 (2015), pp. 054510-1-054510-17.

[34] W. L. McMillian, Transition Temperature of Strong-Coupled Superconductors, Phys. Rev. B 167 (1975) pp. 331–344.

[35] P. B. Allen and R. C. Dynes, Transition temperature of strong-coupled superconductors reanalyzed, Phys. Rev. B 12 (1975) pp. 905–922.

[36] W. Voigt, Lehrbuch der Kristallphysik, Leipzig, Taubner, (1928).

[37] A. Reuss, Berechnung der Fliegrenze von Mischkristallen auf Grund der Plastizittsbedingung fr Einkristalle, Z. Angew. Math. Mech. 9 (1929) 49.

[38] R. Hill, The elastic behaviour of a crystalline aggregate, Proceedings of the Physical Society. Section A 65 (1952) 349-354.

[39] S. F. Pugh, Relations between the elastic moduli and the plastic properties of polycrystalline pure metals, Philos. Mag. 45 (1954) 823.

[40] J. Haines, J. M. Leger, G. Bocquillon, Synthesis and design of superhard materials, Annu. Rev. Mater. Res. 31 (2001) p. 1.

[41] O. L. Anderson, A simplified method for calculating the Debye temperature from elastic constants, J. Phys. Chem. Solids 24 (1963) pp. 909–917.

[42] H. M. Tütüncü, S. Bağcı, G. P. Srivastava and A. Akbulut, Electrons, phonons and superconductivity in rocksalt and tungstencarbide phases of CrC, J. Phys.: Condens. Matter 24 (2012) 455704.

[43] H. M. Tütüncü and G. P. Srivastava, Phonon anomalies and superconductivity in the Heusler compound YPd_2Sn, J. Appl. Phys. 116 (2014) 013907.

[44] H. M. Tütüncü, Ertuğrul Karaca and G. P. Srivastava, Electronphonon interaction and superconductivity in the borocarbide superconductor, Philos. Mag. 97 2669 (2017).

[45] S. Baroni, P. Giannozzi, E. Isaev, Density-functional perturbation theory for quasi-harmonic calculations, Mineral. Geochem. 71 (2010) 39-57.

[46] Y. Wang, J. J. Wang, H. Zhang, V. R. Manga, S. L. Shang, L.-Q. Chen, and Z.-K. Liu, A first-principles approach to finite temperature elastic constants, J. Phys.: Condens. Matter 22 (2010) 225404.

Table 1
Lattice parameters (a, c), bulk modulus (B), its pressure derivative ($B^{'}$) for BaPtSb and and their comparison with previous experimental data.

Source	$a(\AA)$	c ($\AA$)	B (GPa)	$B^{'}$
This work	4.609	4.960	53.0	3.76
Experimental [23]	4.535	4.884		

Table 2
The calculated values of second order elastic constants (C_{ij} in GPa) with and without SOC for the hexagonal BaPtSb.

Method	C_{11}	C_{12}	C_{13}	C_{33}	C_{44}	C_{66}
With SOC	110.32	72.78	32.57	64.94	21.99	32.57
Without SOC	115.06	71.14	32.18	66.79	21.82	31.18

Table 3
The calculated values of isotropic bulk modulus B_{VRH}, shear modulus G_{VRH}, Young's modulus E (all in GPa), B_H/G_H ratio and Poisons's ratio ν with and without SOC for BaPtSb, devired from the corresponding second order elastic constants C_{ij}.

Method	B_V	B_R	B_H	G_V	G_R	G_H	E	B_H/G_H	ν
With SOC	62.38	53.47	57.92	22.39	21.21	21.80	58.12	2.66	0.33
Without SOC	63.10	54.25	58.68	23.88	22.81	23.34	61.83	2.51	0.32

Table 4
The calculated values transverse (V_T), longitudinal (V_L), average elastic wave velocities (V_M) and Debye temperature (Θ_D) with and without SOC for the hexagonal BaPtSb. The experimental value of Debye temperature is also given for comparison.

Method	V_T (m/s)	V_L (m/s)	V_M(m/s)	Θ_D (K)
With SOC	1624.76	3245.49	1822.55	174
Without SOC	1681.21	3297.48	1883.78	179
Experimental [22]				186

Table 5
The calculated values of the physical quantities connected to superconductivity in the noncentrosymmetric BaPtSb superconductor with and without SOC. The available experimental results are also presented for comparison.

Source	N(E_F) (States/eV)	ω_{ln} (K)	λ	$\gamma(\frac{mJ}{molK^2})$	Θ_D (K)	T_c (K)
This work with SOC	1.87	80.73	0.629	7.16	184	1.54
This work without SOC	1.80	82.21	0.617	6.83	182	1.46
Experimental [22]				6.86	186	1.64

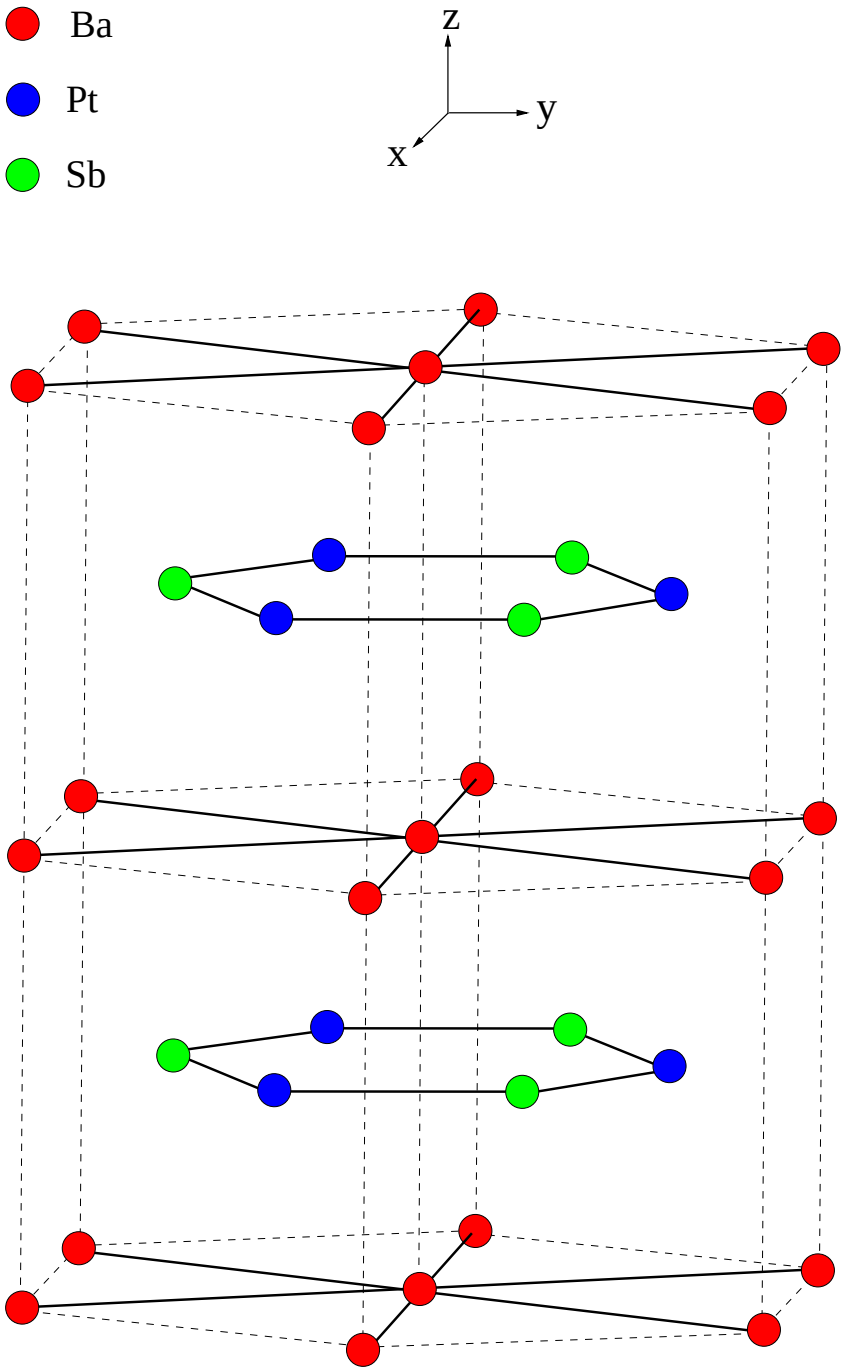

Fig. 1. The hexagonal SrPtSb-type crystal structure of BaPtSb. The structure is composed of a PtSb ordered honeycomb network that stacks along the z-direction so that spatial inversion symmetry is broken globally.

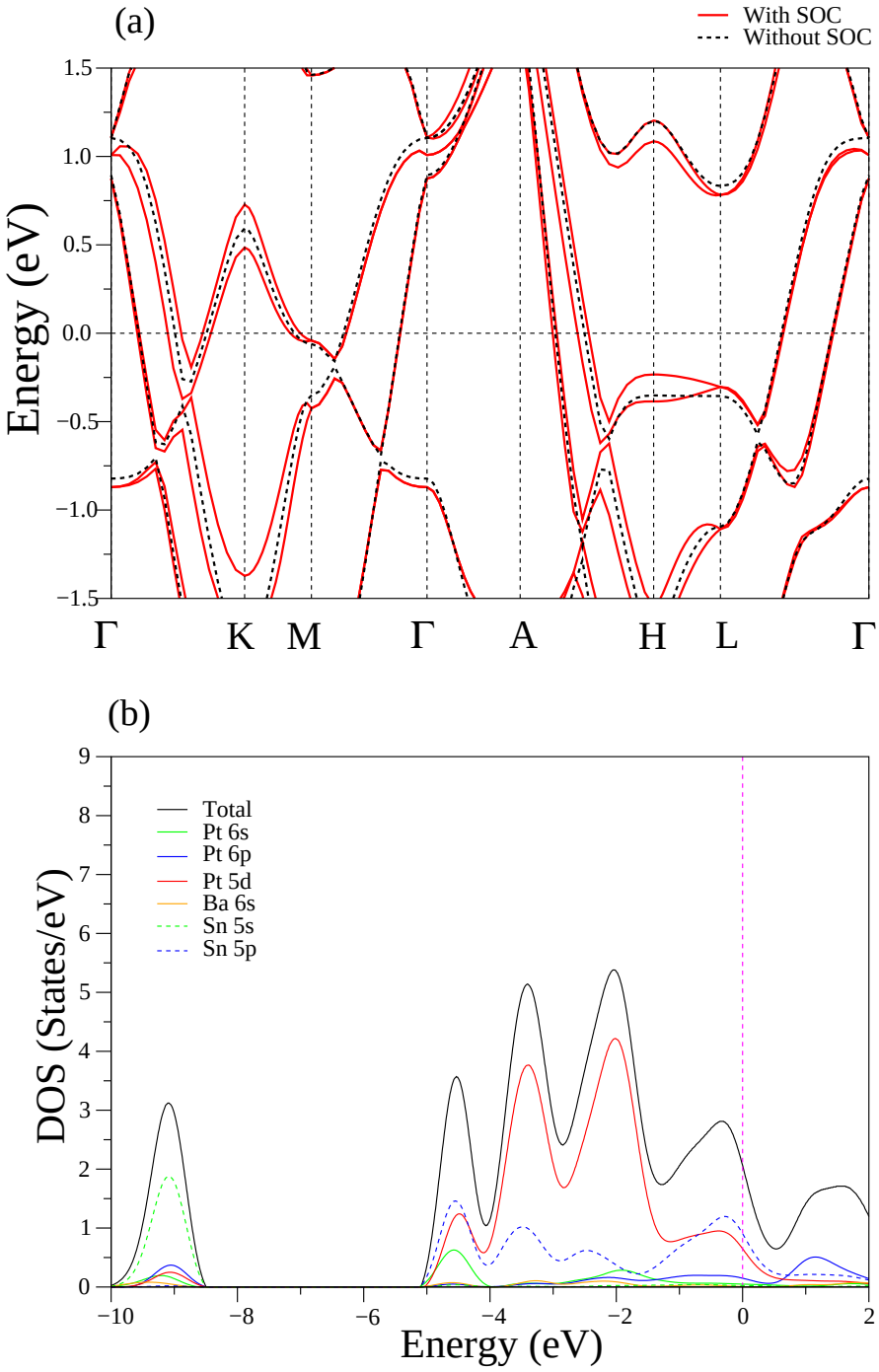

Fig. 2. (a) The calculated electronic band structure of hexagonal BaPtSb with and without SOC along the high symmetry directions in the first Brillouin zone of hexagonal lattice. (b) The calculated total and partial electronic density of states for BaPtSb with SOC.

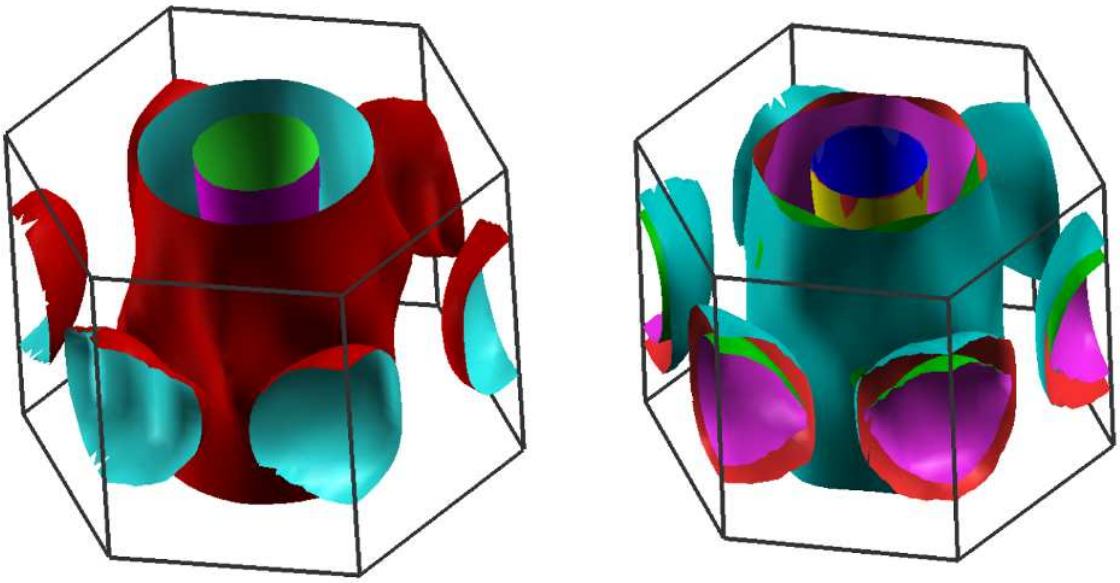

Fig. 3. The calculated Fermi surfaces for hexagonal BaPtSb with(right panel) and without(left panel) SOC.

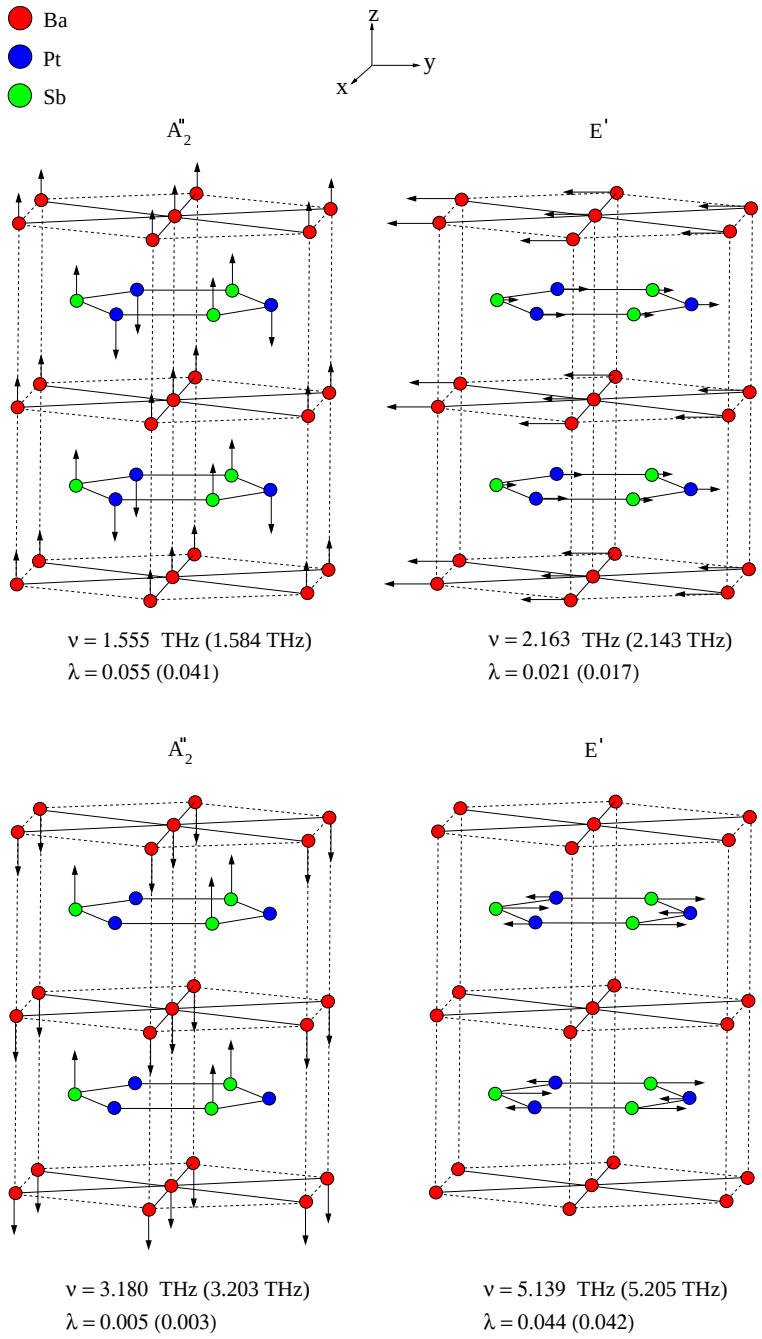

Fig. 4. Eigen atomic displacement patterns for the zone-center modes in BaPtSb. The corresponding results for the zone-center phonon frequencies and their electron-phonon coupling parameters without SOC are presented in the brackets.

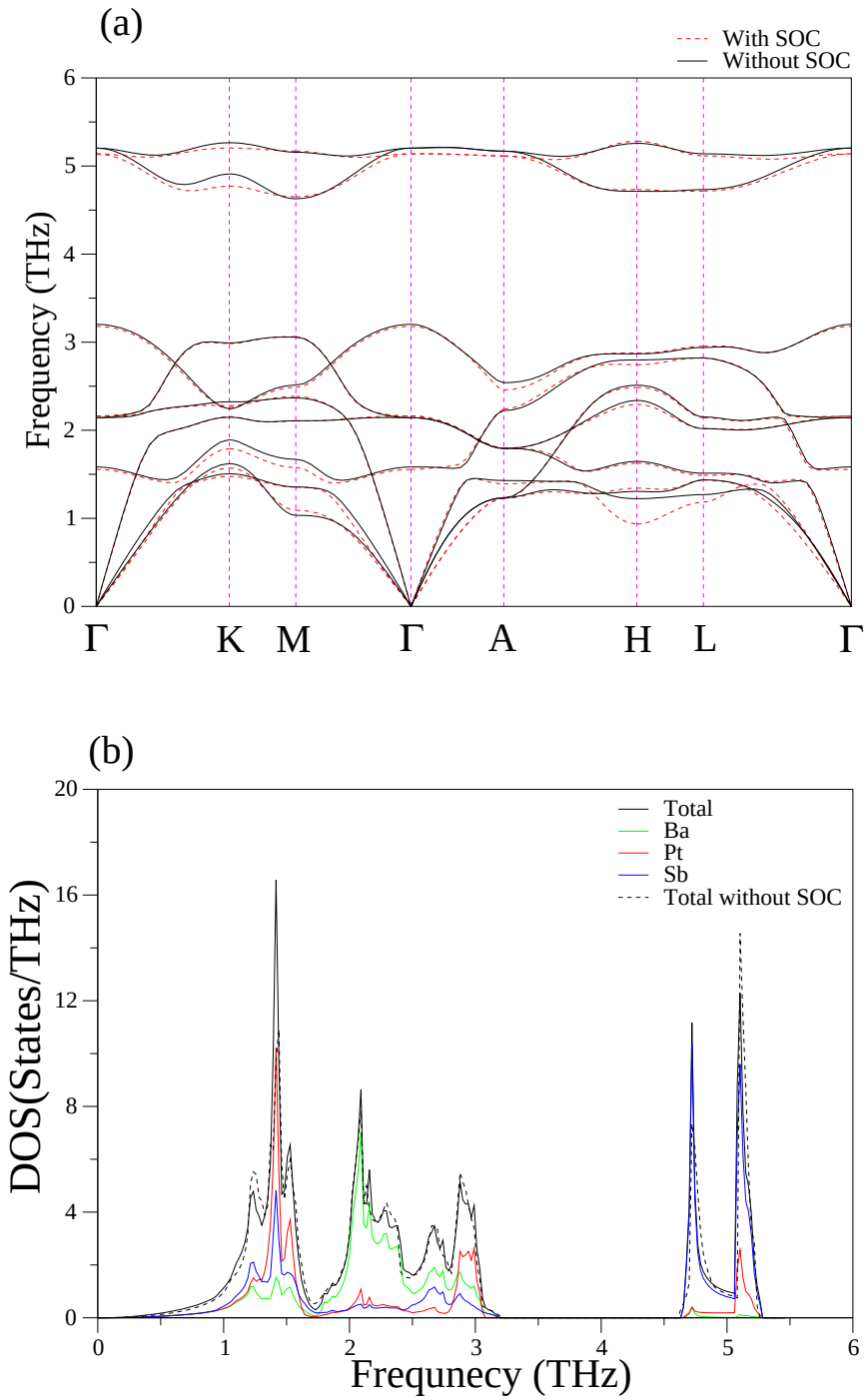

Fig. 5. (a) The calculated phonon dispersion curves of hexagonal BaPtSb with and without SOC along the high symmetry directions in the first Brillouin zone of hexagonal lattice. (b) The calculated total and partial phonon density of states of BaPtSb with SOC.

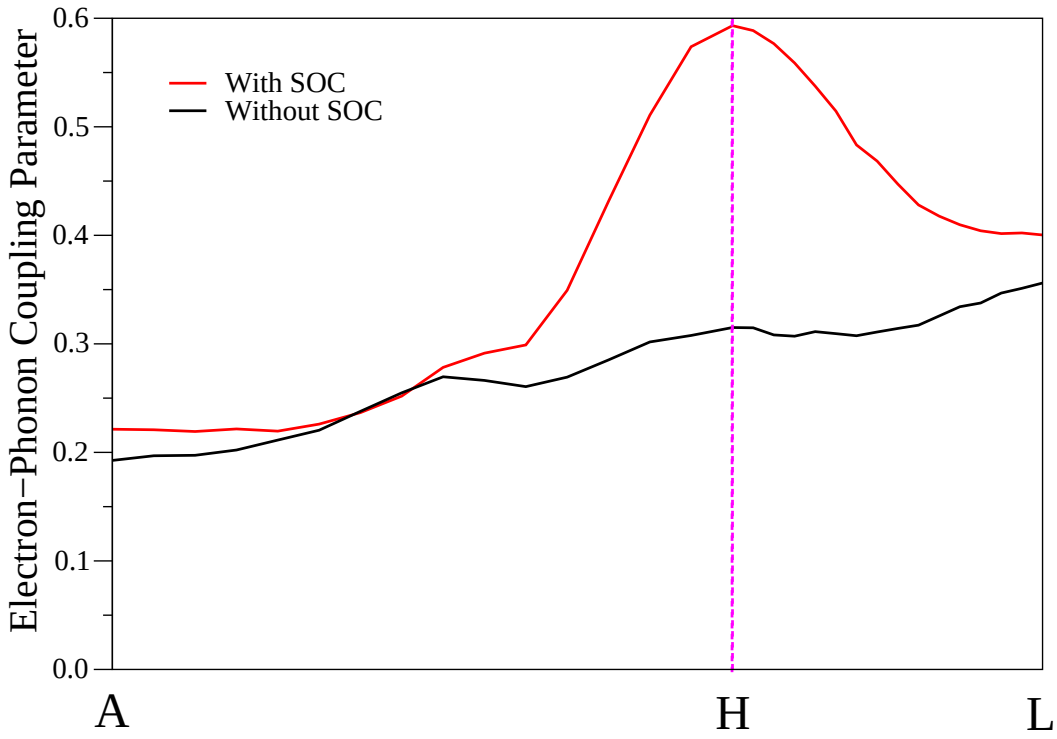

Fig. 6. The frequency variation of electron-phonon coupling parameter for the longitudinal acoustic branch (LA) of BaPtSb along the A-H-L symmetry direction.

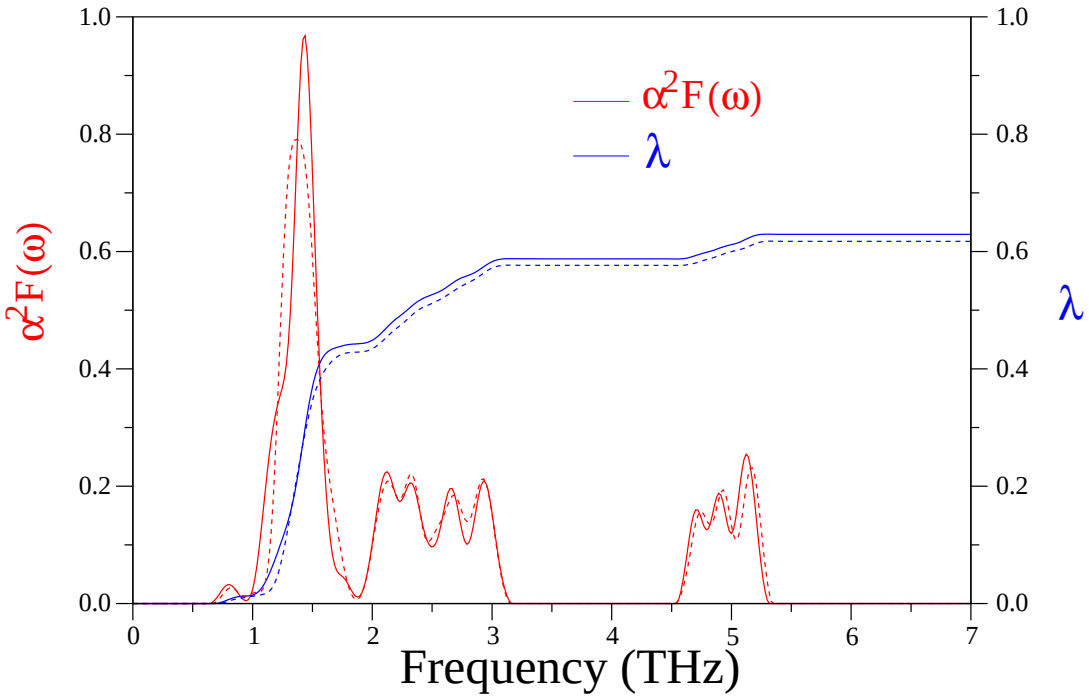

Fig. 7. Eliashberg spectral function $\alpha^2\mathrm{F}(\omega)$ (red line) and integrated electron-phonon coupling parameter λ (blue line) for BaPtSb. The corresponding results without SOC are shown by dashed curves.